Mark J. Jackson · Waqar Ahmed *Editors*

Micro and Nanomanufacturing Volume II

Springer

Micro and Nanomanufacturing Volume II

Mark J. Jackson • Waqar Ahmed
Editors

Micro and Nanomanufacturing Volume II

Springer

Editors
Mark J. Jackson
School of Interdisciplinary Studies
Kansas State University
Manhattan, KS, USA

Waqar Ahmed
School of Mathematics and Physics
University of Lincoln
Lincoln, UK

ISBN 978-3-319-67130-7 ISBN 978-3-319-67132-1 (eBook)
DOI 10.1007/978-3-319-67132-1

Library of Congress Control Number: 2006932032

Printed on acid-free paper

This Springer imprint is published by Springer Nature
The registered company is Springer International Publishing AG
The registered company address is: Gewerbestrasse 11, 6330 Cham, Switzerland

Contents

Chapter 1
Aligned Nanowire Growth

V. Cientanni, W.I. Milne, and M.T. Cole

With many thousands of different varieties to date, the nanowire (NW) library continues to grow at pace. With the continued and hastened maturity of nanotechnology, significant advances in materials science have allowed for the rational synthesis of a myriad of NW types of unique electronic and optical properties, allowing for the realisation of a wealth of novel devices, whose use is touted to become increasingly central in a number of emerging technologies. Nanowires, structures defined as having diameters between 1 and 100 nm, provide length scales at which a variety of inherent and unique physical effects come to the fore [1], phenomena which are often size suppressed in their bulk counterparts [2–4]. It is these size-dependent effects that have underpinned the growing interest in the growth and fabrication, at ever more commercial scales, of nanoscale structures. Nevertheless, many of the intrinsic properties of such NWs become largely smeared and often entirely lost, when they adopt disordered ensembles. Conversely, ordered and aligned NWs have been shown to retain many such properties, alongside proffering various new properties that manifest on the micro- and even macroscale that would hitherto not occur in their disordered counterparts.

V. Cientanni and M.T. Cole contributed equally to this work.

V. Cientanni
Electrical Engineering Division, Department of Engineering, Cambridge University, Cambridge, UK

W.I. Milne
Electrical Engineering Division, Department of Engineering, Cambridge University, Cambridge, UK

Quantum Nanoelectronics Research Center, Tokyo Institute of Technology, Okayama, Tokyo, Japan

M.T. Cole (✉)
Department of Electronic & Electrical Engineering, University of Bath, Bath, UK
e-mail: M.T.Cole@bath.ac.uk

M.J. Jackson, W. Ahmed (eds.), *Micro and Nanomanufacturing Volume II*,
DOI 10.1007/978-3-319-67132-1_1

Nanotechnology is already beginning to present itself as a catalyst for change in many industries and commercial sectors, from nanoparticles in sunscreen [5] to nanotube-infused composites in bicycles [6]. Industries are increasingly commercialising nanomaterials, principally because of the opportunities that occur by downsizing existing microstructures and also because of the many advantages that nanostructures afford. The electronics industry is perhaps one of the best examples of how nanostructures have revolutionised computing. Moore's Law [7] captured the near-annual exponential performance gains from computer processing power, but this stimulus has also demanded increased storage capacity and high-resolution displays, alongside reduced power consumption. All of these aspects of computing have benefited from nanotechnology and the continued miniaturisation to the current 14-nm node due to progressive improvements in top-down conventional Si processing procedures. Almost exclusively, across all technologies, the continued quest for performance improvements rests on engagement with increasingly miniaturised engineering.

NW alignment remains a critical component in the development chain. Alignment underpins much of the success of NW integration into many devices, particularly in the electronics and optics industries. More complicated structures, with potential 3D integration thereafter, such as vertical field-effect transistors [8], room temperature UV nanowire lasers [9], integrated circuits [10], solar cells [11], displays [12] and biosensors [13], have all been shown to benefit greatly from alignment of their consistent nanocomponents. Although the amorphous, disorder ensemble growth of 1D nanostructures has been well documented [14], the focus of this chapter is on the aligned growth of NWs.

Aligned 1D nanostructures, wires, belts, rods and tubes [15], are herein termed NWs. NWs have been extensively studied these past two decades, with particular attention given to carbon nanotubes (CNTs) [16] and semiconducting NWs [17]. Though free-standing-aligned NWs have been reported [18], most practical applications of aligned nanostructures typically require a substrate on to which to adhere and are therefore either grown aligned directly on the substrate (in situ) or are aligned post-growth (ex situ) [19]. Broadly, alignment is either perpendicular (vertical) or parallel (horizontal) to the substrate plane. The reproducible production of horizontally aligned NWs has proven particularly challenging, principally due to the nature of the growth processes involved [20]. The vast wealth of literature on CNTs however, both vertically and horizontally aligned (VA-CNTs and HA-CNTs), warrants dedicated discussion which we will consider latterly in the chapter. Nanostructure alignment methods tend to vary between material types, with similar methods (such as chemical vapour deposition, CVD) differing, often dramatically so, between materials. This chapter does not aim to provide a concise overview of the varied nanomaterial production processes; such a review would be prohibitive in scope. Rather, here we discuss the vertical alignment of the three key NW classes that are central to the fabrication of field-effect transistors, namely, NWs that are either metallic, semiconducting or insulating. We also consider the newly emerging class of inorganic NWs, alongside the more established organic NW family (viz. the carbon nanotubes and nanofibres). In each class we consider

only the most common NW types. For the outlined NW types, we explore the production methods, as well as examining the principle growth mechanisms, the degree of alignment and linear packing densities associated with each.

Following the seminal NW synthesis studies in the late 1990s, various growth kinetics have since been reported. Though a great many varied growth models have been proposed, the most popular growth methods typically adopt vapour–liquid–solid (VLS) growth-based approaches. Traditionally, this mechanism involves three components, a substrate (upon which the NWs are grown), a catalyst (which mediates NW nucleation) and a precursor media (which serves as the NW feedstock). To best outline a general NW growth, here we overview the growth of Si NWs, a prototypical system whose general process flow is, at least in part, applicable to most currently available NW types. In most cases, standard crystalline Si substrates are employed as the growth support, with, in the case of Si NW growth, a gold catalyst deposited by physical vapour deposition (often by sputtering, thermal or electron beam deposition techniques) onto its surface. By increasing the temperature to the substrates eutectic point, a surface alloying between the Au-Si occurs, and the resulting phase becomes liquid. In the case of Si NWs, the precursor gas is typically silicon tetrachloride ($SiCl_4$) or silane (SiH_4). These gaseous molecules disassociate into their constituent components on contact with the liquid catalyst. The liquid catalyst, following some process-specific critical time, becomes supersaturated with dissociated Si. Precursor disassociation continues despite the supersaturated liquid catalyst, resulting in the extrusion or 'freezing' out formation of crystalline Si NWs [21].

CVD and functionally similar reactors are some of the most popular methods for implementing Si NW growth [22–24]. Unconventional VLS has also been demonstrated via oxide-assisted growth, where oxides play an important role in the nucleation and growth instead of more conventional metallic catalysts [25]. The field continues to grow. With ever finer in situ metrology being reported, a greater understanding of the growth kinetics is coming increasingly into focus. Other growth mechanisms for Si NWs have been reported, analogous to the VLS mechanism is the solid-liquid-solid (SLS) and vapour–solid–solid (VSS) growth mechanisms [26, 27]. Figure 1.1 illustrates the key features of the VLS and VSS growth mechanisms.

1.1 Metallic NWs

A wide range of metallic NWs have been produced to date. Of the more than 90 metallic elements, only around 20% have been synthesised into pure metallic NWs, including Ni [28], Co [29], Cu [30], Fe [31], Ni [32], Mo [33], Al [34], Au [35], Ag [36], Zn [37], Sn [38], Na [39] and Mg [40]. A similarly wide variety of alloyed NWs have also been reported, with Ni variants dominating this space, including NiCo [41], NiTi [42], NiAu [43], NiCu [44], PtCu [45], $In_xGa_{1-x}P$ [46] and YFe [47]. Though varied, of these alloyed and pure metallic NWs, it is gold and

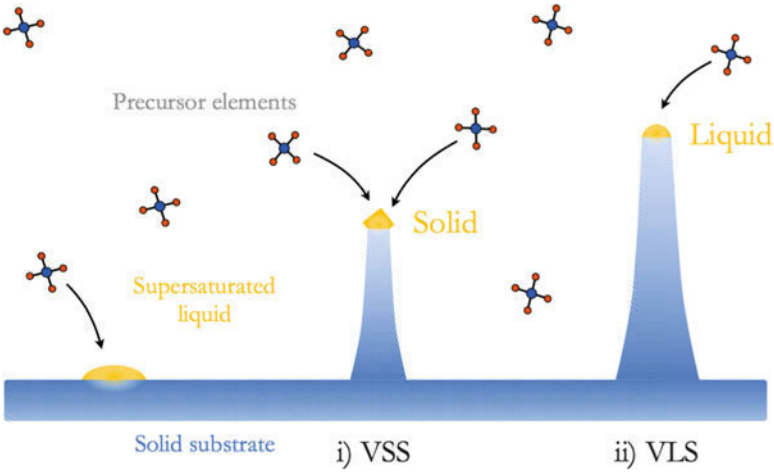

Fig. 1.1 *NW Growth*. Scheme depicting vapour–solid–solid (VSS) and vapour–liquid–solid (VLS) growth regimes. (i) VSS growth occurs at typically lower temperature with a solid catalyst forming on the nanowire tip, whilst (ii) VLS occurs at higher temperature, with the catalyst in the liquid phase

silver NWs that have gleaned perhaps the most attention, in part due to their particularly high electrical and thermal conductivities, facile self-assembly and biocompatibility, all of which have resulted in a breadth of applications, from microelectronics to biosensing [48, 49].

Gold NWs [35, 48–59] are typically prepared from either the self-assembly of gold nanoparticles (bottom-up approach) or from the downscaling or etching of larger systems (top-down approach). The former is typically more popular due to its practicality and scalability and can involve either templated or template-less methods to produce aligned NWs. Here such templates control the NWs direction of growth, often using a porous membrane which serves as a rigid aligning scaffold. There are many soft and hard template methods [52, 56]; however, for aligned gold NWs, hard templates are almost invariably used. A porous anodic aluminium oxide (AAO) or polycarbonate (PC) template is submerged in a solution containing gold nanoparticles which are electrochemically deposited to form NWs [35, 53, 55, 57]. The template is subsequently removed, via etching techniques, leaving vertically aligned NWs. Figure 1.2a shows a typical scanning electron micrograph of vertically aligned Au NWs. Some of the most aligned and densely packed NW forests have been generated by patterning the substrate with either catalysts or pores in some way to introduce isometry to what is an otherwise inherently anisotropic substrate on an atomic level.

Another popular method for synthesising gold NWs is by dielectrophoresis. By applying a potential difference across two electrodes submerged within a gold-containing solution (such as $HAuCl_4$ in n-hexane), NWs grow between the contact electrodes [58, 59]. This powerful method allows accurate control over the macro-scale shape of the NWs with the NW placement dictated by the plating solution.

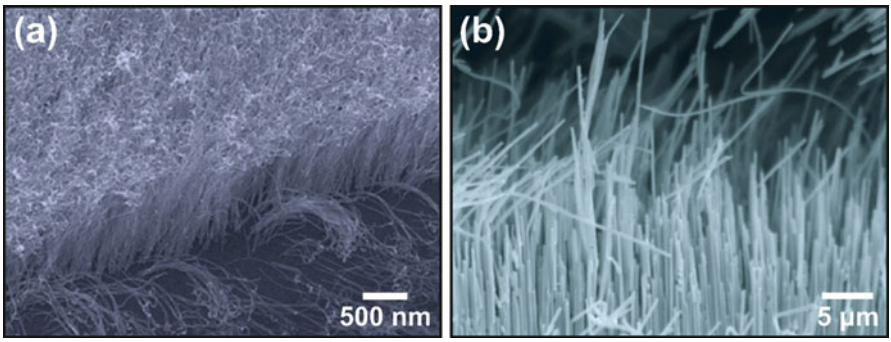

Fig. 1.2 *Metallic NWs*. Example scanning electron micrographs of (**a**) Au NW growth in a polar solution of 4-mercaptobenzoic acid and Au seeds anchored on oxide substrates to catalyse growth of vertically aligned ultrathin Au NWs with 6 nm diameter [51]. (Scale bar, 500 nm) (Copyright American Chemical Society, 2013). (**b**) Ag NW arrays demonstrating concurrent high aspect ratio and high packing density, produced using potentiostatic electrodeposition within confined nanochannels of a commercial porous anodic aluminium oxide (AAO) template [64] (Scale bar, 5 μm) (Copyright Elsevier, 2009)

Nevertheless, the growth of individual NWs is often sporadic, with little to directionality in their growth. The spacing between electrodes has been shown to affect the areal packing density and the degree of alignment. Closely spaced electrodes tend to produce higher degrees of alignment. Higher voltages tend to decrease the time required to align the NWs but also stimulate the formation of larger Au nanoparticles and polycrystalline NWs.

Silver NWs [36, 60–70] have also been widely researched with fervour. Of all the transition metals, silver offers one of the highest electrical conductivities, whilst concurrently exhibiting excellent thermal transport. Figure 1.2b shows a typical scanning electron micrograph of vertically aligned Ag NWs. Nanostructured silver surfaces have also been shown to mediate enhanced Raman scattering for the identification and study of surface-bound molecules, and they have subsequently become particularly attractive as mediators for surface-enhanced Raman spectroscopy. Many methods exist to produce silver NWs. As with gold, silver NW synthesis can be broadly subdivided into template-assisted or template-less methods. The templates are often hard, porous structures, such as polymers, silicon wafers and anodic aluminium oxide (AAO), whereas template-less approaches follow a ‘soft solution’ method, involving the surfactant-assisted reduction of silver oxide with platinum seeds (termed the polyol method) [36, 60].

1.2 Semiconducting NWs

Since some of the first studies on the synthesis of nanowhiskers by Hitachi in the early 1990s [71], the field of semiconducting NW growth has developed at an unusually fast pace. Including direct and indirect, as well as pure and compound,

there are more than 130-bulk semiconducting systems known. Of these, but a few semiconducting NWs—including single component, compound, functional oxides, nitrides and carbides—have been synthesised, including IV–IV Group, Si [72], Ge [73] and $Si_{(1-x)}Ge_x$; III–V Group (binary), InP [74], lnAs [71], GaAs [75] and GaP [76]; III–V Group (ternary), $Ga(As_{(1-x)}P_x)$ [77], $ln(As_{(1-x)}P_x)$ [78], $(Ga_{(1-x)}ln_x)P$ [79], $(Ga_{(1-x)}ln_x)As$ [80] and $(Ga_{(1-x)}ln_x)(As_{(1-x)}P_x)$ [81]; II–VI Group (binary), ZnS [82], ZnSe [83], CdS [84] and CdSe [85]; IV–VI Group (binary), PbSe [86], Bi_2Te_3 [87] and PbTe [87]; as well as the nitrides and carbides, GaN [88], Si_xN_y [89] and SiC [90] and the functional oxides, ZnO [37], TiO_2 [91], SnO_2 [92], CuO [93] and In_2O_3 [94]. Of these, Si has been at the centre of study for many decades and represents a prototypical growth system on which many of the latterly demonstrated alloyed NWs have been based.

Si NWs [17, 21–27, 72, 95–105] have been researched for nearly 60 years; although in truth, the wires produced in 1957 by Treuting et al. were not what we would now strictly classify as NWs due to their overly large diameter [98]. Following a hiatus in research, a reinvigorated research community gave rise to a sprawl of publications since the turn of the millennium, principally in light of advances in ever more miniaturised microelectronics. Morales et al., in 1998, published one of the first reports on truly nanoscale Si NW [100], introducing controlled laser ablation to the wider materials community. Today Si NWs are still extensively researched due to their potential use in computing and microelectronic applications. Aside from CVD, other reported experimental growth systems for the synthesis of aligned Si NWs include reactive atmospheric annealing [105], evaporation of SiO [99], solution-based [72] and laser ablation [95]. Figure 1.3a shows a typical scanning electron micrograph of vertically aligned Si NWs.

Due to its high compatibility with Si-based technologies, Ge has also been researched at length. Figure 1.3b shows a typical scanning electron micrograph of vertically aligned Ge NWs. Ge has some important advantages over Si, in particular it's higher charge carrier mobility and larger Bohr exciton radius. Ge NWs have been successfully integrated in lithium-ion batteries [106], field-effect transistors [107], computing memory [108] and many optoelectronic applications [109]. Based on established VLS kinetics, Ge is typically synthesised using systems similar to those used for Si, with CVD and MO-CVD dominating this space, along with molecular beam epitaxy (MBE), and template methods being some of the most popular techniques.

Together with the arguably more conventional Si and Ge, ZnO is one of the most widely studied semiconducting NWs due to its wide band gap, high electron mobility, high room temperature luminescence and high optical transparency [37]. ZnO has been favoured for photodetectors and sensors to, more recently, UV lasers. Figure 1.3c shows a typical scanning electron micrograph of vertically aligned ZnO NWs. Typical production methods include thermal evaporation, MO-CVD (metal-oxide assisted), high-pressure laser ablation and aqueous synthesis (including hydrothermal). Sol–gel processes have also been demonstrated. Typically used for the fabrication of metal oxides of Si and Ti, sol–gel approaches have proven to be extremely popular. Here monomers are converted into a colloidal

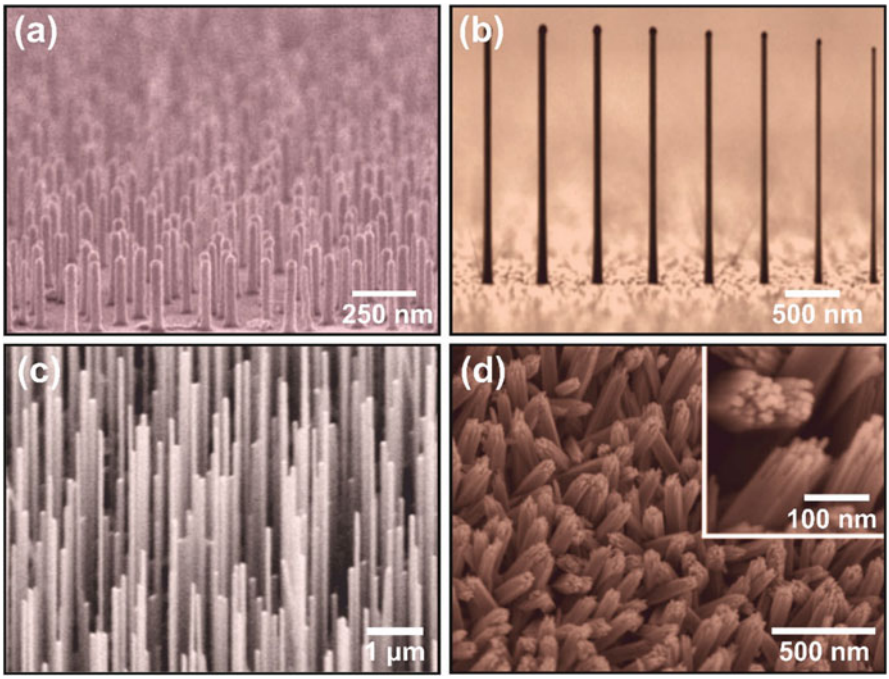

Fig. 1.3 *Semiconducting NWs*. Example scanning electron micrographs depicting the (**a**) effect of growth temperature on the tapering of Si NWs by epitaxial vapour–solid–solid growth via Al-catalysis [27]. (Scale bar, 250 nm) (Copyright Nature Publishing Group, 2006). (**b**) A linear array of Ge NWs grown from lithographically patterned Au catalyst dots. Note the systematic reduction in NW length with decreasing diameter (*left* to *right*) [191] (Scale bar, 3 μm) (Copyright ACS Publications, 2010). (**c**) VLS growth of highly aligned vertical ZnO NWs, grown using a 5 nm Au catalyst [192] (Scale bar, 500 nm) (Copyright Hindawi Publishing Corporation, 2012). (**d**) A scanning electron micrograph of TiO_2 NWs grown in an atmospheric glass vessel, using 0.3 mL $TiCl_3$ and 15 g lauric acid [114] (Scale bar, 1 μm) (Copyright Nature Publishing Group, 2015)

diphase solution which is a precursor for a generated particulate/polymer network, termed the 'gel'. In order to form aligned NWs, in situ, this method is often combined with AAO or similar hard templating techniques [110]. The comparatively low-cost and simple experimental setups associated with hydrothermal and sol–gel techniques have made them especially prevalent in growing research communities.

Wide band gap TiO_2 NWs have shown varied unique solid state chemical and physical properties. Their applications range from electrodes in lithium-ion batteries and fuel cells to hydrogen production and containment, photovoltaics and supercapacitors [111, 112].

Titanium dioxide is generally compatible with CVD, electrochemical tempting and solvo−/hydrothermal techniques. Hydrothermal/solvothermal synthesis methods are normally performed in high-pressure stainless steel vessels

(or Teflon reactors) termed autoclaves. Using substrates such as indium tin oxide (ITO), Si/SiO_2 or glass, an aqueous solution is prepared, and the substrates submerged. The solution often contains a titanium precursor and a strong solvent such as hydrogen chloride. The experimental procedure requires a temperature higher than the boiling temperature of the solvent, which limits their safety and makes large-scale production challenging. Typical hydrothermal synthesis of TiO_2 nanowires requires high concentrations of either strongly base or strongly acidic environments, which results in equipment corrosion, produces volatile waste products and significant issues surrounding process safety, viability and scalability [91, 113].

Surface-limited reaction CVD is popular for TiO_2 synthesis; however, large-scale production has proven problematic due to the high melting point and very low vapour pressure of Ti. The resulting deposition window is small and selective, confining the crystalline nature of the formed NWs [111]. A novel method capable of achieving alignment with high packing densities has been reported, involving low temperature and atmospheric pressure mixing of titanium oxide with fatty acids. Self-hydrolysis, nucleation and crystallisation result in a sealed vial, at room temperature. The NWs can be easily fabricated by careful manipulation of the saturated fatty acids [114].

1.3 Dielectric NWs

Various dielectric nanowires have been reported, including MgO [115], Si_3N_4 [116], SiO_2 [117], Al_2O_3 [118], NiO [119–126], BN [127–136] and WO [137]. Figure 1.4 shows typical scanning electron micrographs of vertically aligned SiO_2 and Si_3N_4 NWs. Ambient pressure, high-temperature thermal annealing has been widely used to synthesise stoichiometric dielectric NWs. Of these Si_3N_4 and *a*-SiO_2 NWs have been demonstrated, with yields and morphologies which show a clear dependence on the flow rates of the gaseous reactants [116]. In the case of SiO_2 NWs, one-pot electrospinning is gaining significant traction due to its low cost and potentially high throughput [138]. Aerosol-mediated spontaneous SiO_2 NW growth via flame spray pyrolysis of organometallic solutions (hexamethyldisiloxane or tetraethyl orthosilicate) has shown potential, though low yields and scale-up issues make the approach otherwise commercially challenging; nevertheless, compatibility with a range of substrates has been suggested increasing the appeal of the approach [139]. Though various metal-catalysed growths are possible [140, 141], such systems pose clear limitations for the realisation of high dielectric constant NWs. Catalyst attrition during growth and sub-nm metallic remnants along the NWs length fundamentally limit the usefulness of these techniques in realising high purity dielectric NWs. Pure-metallic-catalyst-free carbothermal reduction of CuO powders under Ar/O_2 flow has been shown to be one possible approach, though extraneous SiC formation must be quenched if commercially viable purities and yield are to be achieved [142]. As with other

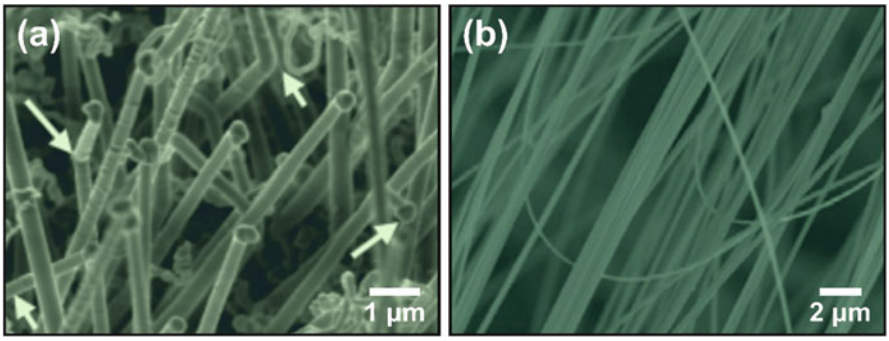

Fig. 1.4 *Dielectric NWs*. Example scanning electron micrographs of (**a**) CVD-synthesised aligned SiO_2 NWs [117] (Scale bar, 1 μm) (Copyright American Chemical Society, 2006). (**b**) Centimetre-long α-Si_3N_4 NWs by template-free pyrolysis of polymeric precursors [193]. (Scale bar, 2 μm) (Copyright Institute of Physics, 2008)

CVD process, though many varied catalysts have demonstrated catalytic potential, the yields of each are extremely varied, with, in most cases, metal catalysts producing some of the highest yields, clearly at the expense of the NWs dielectric properties. This issue similarly plagues SiO_2 NW growth; annealing of SiO catalysts on Si and subsequent growth via SLS proffer an attractive and entirely metal-free system, though extremely low areal yields and very poor alignment limit the approach.

1.4 Inorganic NWs

Inorganic molecular NWs have emerged as a new material with radically new functional properties, particularly molybdenum halide and the chalcogenide polymers, along with various other molybdenum chain-based variants. These 1D polymers behave distinctly from CNTs and other NWs, demonstrating anionic bridges with high strength, non-Newtonian mechanical properties and remarkably high Young's moduli [143]. Molecular NWs of the form $Mo_6 S_{9-x} I_x$ (herein MoSI) have been identified as some of the most promising within the wider NW family, with the ability to form bundles with air-stable single wire dispersions, high scalability and reproducibility [144–146].

Typically, MoSI molecular NWs are formed in a sealed and evacuated quartz ampoule, containing metallic Mo platelets, placed in a single zone furnace at approximately 1000 K, with some annealing the samples for up to 72 h. This creates fur-like NWs, with high mechanical strength and toughness [144, 147]. Bundles can have lengths of over 5 mm; however, shear and mechanical exfoliation of the bundles is simple due to the relatively low inter-wire Van der Waals forces. Alongside this furnace method, hydrothermal/solvothermal methods are also becoming increasingly routine for producing MoSI NWs, with reasonably high

alignment and high linear packing density. Another production route is via soft lithography using PDMS micromolds. Here, networks are created in which the NWs grow, between a substrate such as silicon or glass and the micromold. Dissolving single crystals of $LiMo_3Se_3$ in polar solvents, such as dimethyl sulfoxide or *N*-methylformamide, are then used to form individual MoSe NWs [148, 149]. The attainable packing density associated with these methods is limited by the resolution obtainable on the stamp between individual trenches. Nevertheless, such stamping techniques tend to produce NWs with excellent alignment as the NWs tend to form in the predetermined channels. Low packing densities are common, though high NW linearity and degree of alignment are often evidenced, with reasonable reproducibility compared to other methods, such as optical lithography which is otherwise well established and widely accepted.

1.5 Organic NWs

Carbon nanotubes (CNTs) are an important member of the NW family. CNTs are seamlessly bonded, rolled sheets of hexagonally latticed carbon atoms consisting of one or more cylindrically nested layers of graphene. Those CNTs consisting of one wall are termed single-walled carbon nanotubes (SWNTs), whilst those with more than one wall are termed multi-walled carbon nanotubes (MWNTs). Since the popularising paper of Iijima in 1991, CNTs have drawn much attention due to their incredible electrical and mechanical properties and wide-ranging potential commercial applications, including the use as electrical conductors, high strength composites, nanosized interconnects and electromagnet shielding (but to name a few) [16, 150]. For many of the mentioned applications, it is highly desirable to produce aligned CNTs (either vertically, VA-CNTs or horizontally, HA-CNTs). The production methods for aligned CNTs are diverse, yielding many different packing densities and degrees of alignment for each method. One of the most popular and scalable methods for producing VA-CNTs is via CVD, with many variants reported, such as water-assisted CVD (WA-CVD) [151], plasma-enhanced CVD (PE-CVD) [152] and photo thermal CVD [153].

Compared to the wider family of NWs, VA-CNTs typically present higher areal packing densities for comparable length scales, along with higher degrees of alignment. CNT forests also tend to be more uniform in nature compared to many other CVD-synthesised NW types. However, at a scale of 2–10 nm (the typical diameter of a SWNT), CNTs tend to afford much less local alignment. SWNTs tend to intertwine and wrap around one another, whereas the wider family of crystalline NWs discussed prior is much more aligned and maintains this alignment across all length scales. Unlike the CNTs, whose morphology can be sinuous and softly varying, any change in growth direction for the majority of NWs tends to be sharp, straight and angular. The issue with isolating individual CNTs and also the loss in the performance of bulk CNTs compared to single tubes currently limits their commercial viability and device performance. VA-CNTs also tend to have less

variance in the alignment and packing density compared to other NW types. This is likely attributed to the fact that CVD methods dominate the research landscape for the production of VA-CNTs, whilst nanowires can be produced with a plethora of methods all yielding different degrees of alignment and nanowire densities. It should also be mentioned that MWNT compared to SWNT tends to present a generally larger degree of vertical alignment and often does not present local spindling.

Horizontally aligned CNTs can be produced in bulk, post synthesis (often from VA-CNT forests), via ex situ alignment. In situ alignment corresponds to manifest directional control during growth. Focussing on in situ, as the literature presented in this chapter thus far has been exclusively directed towards growth methods and hence in situ techniques, there are a number of ways of horizontally aligning CNTs during growth. The three most popular methods used for in situ growth of HA-CNTs are graphoepitaxy (lattice guided), gas flow directed and electric or magnetic field alignment. The first of these methods exploits asymmetries in the atomic lattice of the substrate or through physical contouring of the substrate [154–171]. This method typically presents high alignment, because of the substrates highly orientated lattice. However, the packing density is often reasonably low (10 μm^{-1}). Combined gas flow and lattice orientation have been used to achieve high alignment with high packing densities. CNTs aligned with either magnetic or electric fields require growth to be conducted between magnetic poles or electrodes with an applied external electric field (which can be either DC or AC). Electric field-aligned CNTs often show a degree of variance in both the packing density and alignment, likely attributed to spatial and temporal variations in the aligning field. The alignment is strongly dependent on the strength and direction of the electric field as well as the underpinning growth which augments the local fields during the growth. DC and AC fields have been used, with little correlation to alignment en mass [172–181]. Gas flow alignment involves the flow of gases during growth, typically of the growth precursors, which align the CNTs along the velocity vector of the flowing gas. To increase their alignment, gas flow-aligned CNTs are often dependent upon the kinetics of the predetermined catalyst loaded into the reactor. This explains, at least in part, the variation in the resulting distribution in both packing density and degree of alignment [182–190].

1.6 Degree of Alignment and Linear Packing Density

From the majority of the NW types presented above, we have conducted an outline meta-analysis to evaluate both their linear packing density (NW per μm) and their degree of alignment. Packing density was determined using a quantitative method, by plotting contrast histograms from extracted SEM imagery or from packing densities explicitly quoted. Out of necessity, the degree of alignment (DoA) was assessed qualitatively. As the assessed DoA is scale dependent and as each source image had invariably differing scales, only broad banding of the DoA was possible.

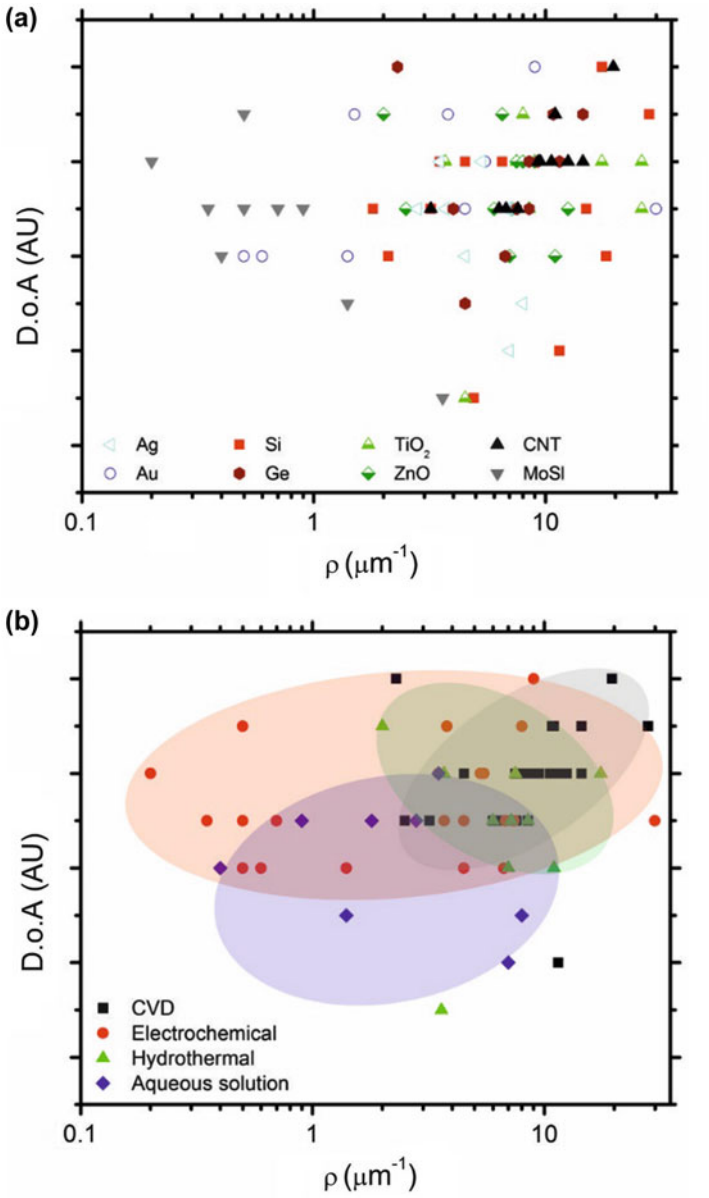

Fig. 1.5 Variation in the degree of alignment (DOA) as a function of linear packing density (ρ), for a select cross-section of the wide class of vertically aligned NWs as a function: (**a**) material (including the metallic NWs, Au [35, 48–59] and Ag [36, 60–70], the semiconducting NWs, Si [17, 21–27, 72, 95–105] and Ge [73, 191, 194–202] and dielectric NWs, TiO_2 [203] and ZnO [60, 110, 192, 203–211]. Also shown are typical organic (CNTs [150–153, 212–219]) and inorganic (MoSI [33, 143–149, 220, 221] NWs) and (**b**) synthesis method. Note the distinct grouping of CVD methods (densely packed and highly aligned) as well as electrochemical templating (high alignment). Hydrothermal methods produce relatively modest packing densities, whilst aqueous solution methods appear to produce relatively low packing density and low alignment

To enhance the rigour of the analysis, a randomly selected partial set of images, all of a comparable length scale, was taken, and the DoA was independently quantified using the image analysis methodology as outlined in [18]. A ranking was thereby generated and compared to our original ranking. The two showed a high correlation, herewith independently confirming our initial ranking.

As shown in Fig. 1.5a, b, the growth technique rather than the NW material tends to dominate the DoA. Etching templating produces NWs with generally high density and with good alignment, with none of the characteristic kinking, or sudden change in direction of growth typical of VLS. Figure 1.5b shows the DoA as a function of linear packing density and growth method. Note the formation of zones coarsely associated with each growth method. Of these, CVD appears to produce growth which tended to have high alignment and high packing density. This is likely due to the nature of the growth, which supports high nucleation and concurrent alignment due to Van der Waals interactions associated with the surrounding NWs. Zoning of the MoSI and broader class of PDMS-printed molecular NWs is evident, with high DoA and low packing density. Other electrochemical methods have produced a range of linear packing densities but almost always give high DoA due to the templating process. Solvo- and hydrothermal methods generally allow for high linear packing densities with a broad range of possible alignments.

1.7 Conclusion

In the present chapter, we have attempted to capture a broad overview of the current status in the field of aligned nanowire growth. Summarising the core nanowire types, we have outlined the leading as well as some of the more exotic growth techniques as they pertain to in situ nanowire alignment. The field is diverse and inevitably governed by the eventual application of the nanoengineered structures. Nonetheless, an inclusive meta-analysis of the present literature suggests that, with the continued miniaturisation of engineering components, CVD techniques allow for controlled alignment and linear packing density and as such represent a clear route to market and an eventual means of gaining commercial traction in the next decade.

References

1. Hornyak GL (2009) Fundamentals of nanotechnology. Taylor & Francis Group, Boca Raton, FL
2. Nalwa HS (2000) Handbook of nanostructured materials and nanotechnology. Academic Press, New York, NY
3. Alivisatos P, Barbara PF, Castleman AW, Chang J, Dixon DA, Klein ML, McLendon GL, Miller JS, Ratner MA, Rossky PJ, Stupp SI, Thompson ME (1998) From molecules to materials: current trends and future directions. Adv Mater 10(16):39

4. Shalaev VM, Moskovits M (1999) Nanostructured materials: clusters, composites, and thin films. American Chemical Society, Washington, DC
5. Smijs TG, Pavel S (2011) Titanium dioxide and zinc oxide nanoparticles in sunscreens: focus on their safety and effectiveness. Nanotechnol Sci Appl 2011(4):17. Dovepress
6. Suhr J et al (2005) Viscoelasticity in carbon nanotube composites. Nat Mater 4(2):134–137
7. Moore GE (1998) Cramming more components onto integrated circuits. Proc IEEE 86(1):4
8. Ng HT et al (2004) Single crystal nanowire vertical surround-gate field-effect transistor. Nano Lett 4(7):1247–1252
9. Huang MH et al (2001) Room-temperature ultraviolet nanowire nanolasers. Science 292 (5523):1897–1899
10. Thelander C et al (2006) Nanowire-based one-dimensional electronics. Mater Today 9 (10):28–35
11. Law M et al (2005) Nanowire dye-sensitized solar cells. Nat Mater 4(6):455–459
12. Sun XW, Wang JX (2008) Fast switching electrochromic display using a viologen-modified Zno nanowire array electrode. Nano Lett 8(7):1884–1889
13. Patolsky F et al (2004) Electrical detection of single viruses. Proc Natl Acad Sci U S A 101 (39):14017–14022
14. Xia Y et al (2003) One-dimensional nanostructures: synthesis, characterization, and applications. Adv Mater 15(5):353–389
15. Wang ZL (2000) Characterizing the structure and properties of individual wire-like nanoentities. Adv Mater 12(17):1295–1298
16. De Volder MFL et al (2013) Carbon nanotubes: present and future commercial applications. Science 339(6119):535–539
17. Schmidt V et al (2009) Silicon nanowires: a review on aspects of their growth and their electrical properties. Adv Mater 21(25–26):2681–2702
18. Cole MT et al (2014) Ultra-broadband polarisers based on metastable free-standing aligned carbon nanotube membranes. Adv Opt Mater 2(10):929–937
19. Zhang Q et al (2016) In situ fabrication and investigation of nanostructures and nanodevices with a microscope. Chem Soc Rev 45(9):2694–2713
20. Ghoshal T et al (2014) Fabrication of ordered, large scale, horizontally-aligned Si nanowire arrays based on an in situ hard mask block copolymer approach. Adv Mater 26(8):1207–1216
21. Wagner RS, Ellis WC (1964) Vapor-liquid-solid mechanism of single crystal growth. Appl Phys Lett 4(5):89–90
22. Ho T-W, Hong FC-N (2012) A reliable method to grow vertically-aligned silicon nanowires by a novel ramp-cooling process. Appl Surf Sci 258(20):7989–7996
23. Hochbaum AI et al (2005) Controlled growth of Si nanowire arrays for device integration. Nano Lett 5(3):457–460
24. Wacaser BA et al (2009) Growth system, structure, and doping of aluminum-seeded epitaxial silicon nanowires. Nano Lett 9(9):3296–3301
25. Zhang R-Q, Lifshitz Y, Lee S-T (2003) Oxide-assisted growth of semiconducting nanowires. Adv Mater 15(7–8):635–640
26. Yan HF et al (2000) Growth of amorphous silicon nanowires via a solid–liquid–solid mechanism. Chem Phys Lett 323(3–4):224–228
27. Wang Y et al (2006) Epitaxial growth of silicon nanowires using an aluminium catalyst. Nat Nanotechnol 1(3):186–189
28. Thongmee S et al (2009) Fabrication and magnetic properties of metallic nanowires via aao templates. J Magnetism Magn Mater 321(18):2712–2716
29. Cantu-Valle J et al (2015) Mapping the magnetic and crystal structure in cobalt nanowires. J Appl Phys 118(2):024302
30. Cui F et al (2015) Synthesis of ultrathin copper nanowires using tris(trimethylsilyl)silane for high-performance and low-haze transparent conductors. Nano Lett 15(11):7610–7615
31. Haehnel V et al (2010) Towards smooth and pure iron nanowires grown by electrodeposition in self-organized alumina membranes. Acta Mater 58(7):2330–2337

32. Kim J et al (2016) Organic devices based on nickel nanowires transparent electrode. Sci Rep 6:19813
33. Zach MP, Ng KH, Penner RM (2000) Molybdenum nanowires by electrodeposition. Science 290(5499):2120–2123
34. Lee JW et al (2010) Single crystalline aluminum nanowires with ideal resistivity. Scr Mater 63(10):1009–1012
35. Dou R, Derby B (2008) The growth and mechanical properties of gold nanowires. MRS Online Proceedings Library Archive. 1086: pp 1086–U08-01 (6 pages)
36. Cao Y et al (2006) A technique for controlling the alignment of silver nanowires with an electric field. Nanotechnology 17(9):2378
37. Chen YJ et al (2007) Controlled growth of zinc nanowires. Mater Lett 61(1):144–147
38. Djenizian T et al (2008) Electrochemical fabrication of tin nanowires: a short review. C R Chim 11(9):995–1003
39. Yanson AI, Yanson IK, van Ruitenbeek JM (1999) Observation of shell structure in sodium nanowires. Nature 400(6740):144–146
40. Li W et al (2007) Magnesium nanowires: enhanced kinetics for hydrogen absorption and desorption. J Am Chem Soc 129(21):6710–6711
41. Thongmee S et al (2009) Unique nanostructures in nico alloy nanowires. Acta Mater 57 (8):2482–2487
42. Hou H, Hamilton RF (2015) Free-standing niti alloy nanowires fabricated by nanoskiving. Nanoscale 7(32):13373–13378
43. Kumar S, Saini D (2013) Large-scale synthesis of Au–Ni alloy nanowires using electrochemical deposition. Appl Nanosci 3(2):101–107
44. Wang CZ et al (2002) Structure and magnetic property of Ni-Cu alloy nanowires electrodeposited into the pores of anodic alumina membranes. J Phys D Appl Phys 35(8):738
45. Liao Y et al (2016) Composition-tunable ptcu alloy nanowires and electrocatalytic synergy for methanol oxidation reaction. J Phys Chem C 120(19):10476–10484
46. Kornienko N et al (2015) Solution phase synthesis of indium gallium phosphide alloy nanowires. ACS Nano 9(4):3951–3960
47. Wang X et al (2016) Preparation and characterization of Y-Fe alloy nanowires by template-assisted electrodeposition from aqueous solution. J Nanopart Res 18(3):1–12
48. Dawson K, Riordan AO (2011) Towards nanowire (bio) sensors. J Phys Conf Series 307 (1):012004
49. Zhang Y et al (2014) New gold nanostructures for sensor applications: a review. Materials 7 (7):5169
50. Chi S, Farias SL, Cammarata RC (2012) Synthesis of vertically aligned gold nanowire-ferromagnetic metal matrix composites. ECS Trans 41(35):119–122
51. He J et al (2013) Forest of gold nanowires: a new type of nanocrystal growth. ACS Nano 7 (3):2733–2740
52. Kline TR et al (2006) Template-grown metal nanowires. Inorg Chem 45(19):7555–7565
53. Liu J et al (2006) Electrochemical fabrication of single-crystalline and polycrystalline au nanowires: the influence of deposition parameters. Nanotechnology 17(8):1922
54. Reinhardt HM, Bücker K, Hampp NA (2015) Directed assembly of gold nanowires on silicon via reorganization and simultaneous fusion of randomly distributed gold nanoparticles. Opt Express 23(9):11965–11974
55. Reynes O, Demoustier-Champagne S (2005) Template electrochemical growth of polypyrrole and gold-polypyrrole-gold nanowire arrays. J Electrochem Soc 152(9):D130–D135
56. Shi S et al (2011) Fabrication of periodic metal nanowires with microscale mold by nanoimprint lithography. ACS Appl Mater Interfaces 3(11):4174–4179
57. Zheng L, Li S, Burke PJ (2004) Self-assembled gold nanowires from nanoparticles: an electronic route towards DNA nanosensors. Proc. SPIE 5515:117–124

58. Venkatesh R et al (2015) Directed assembly of ultrathin gold nanowires over large area by dielectrophoresis. Langmuir 31(33):9246–9252
59. Zhang M et al (2013) Controllable growth of gold nanowires and nanoactuators via high-frequency Ac electrodeposition. Electrochem Commun 27:133–136
60. Lu L et al (2012) Direct synthesis of vertically aligned ZnO nanowires on FTO substrates using a CVD method and the improvement of photovoltaic performance. Nanoscale Res Lett 7(1):1–8
61. Yang R et al (2007) Silver nanowires prepared by modified AAO template method. Mater Lett 61(3):900–903
62. Sun Y et al (2002) Uniform silver nanowires synthesis by reducing AgNO3 with ethylene glycol in the presence of seeds and poly(vinyl pyrrolidone). Chem Mater 14(11):4736–4745
63. Sun Y et al (2002) Crystalline silver nanowires by soft solution processing. Nano Lett 2 (2):165–168
64. Sun B et al (2009) Single-crystal silver nanowires: preparation and surface-enhanced raman scattering (sers) property. Mater Lett 63(29):2570–2573
65. Mohammad A et al (2014) Optical characteristics of vertically aligned arrays of branched silver nanowires. 14th IEEE international conference on nanotechnology, pp 563–566
66. Malandrino G, Finocchiaro ST, Fragala IL (2004) Silver nanowires by a sonoself-reduction template process. J Mater Chem 14(18):2726–2728
67. Kazeminezhad I et al (2007) Templated electrodeposition of silver nanowires in a nanoporous polycarbonate membrane from a nonaqueous ionic liquid electrolyte. Appl Phys A 86 (3):373–375
68. Han Y-H (2008) High density silver nanowire arrays using self-ordered anodic aluminum oxide (AAO) membrane. J Korean Ceramic Soc 45(4):191–195
69. Chun-Nuan Y et al (2004) Growth mechanism of vertically aligned Ag(TCNQ) nanowires. Chin Phys Lett 21(9):1787
70. Cao Y, He J, Sun J (2009) Fabrication of oriented arrays of porous gold microsheaths using aligned silver nanowires as sacrificial template. Mater Lett 63(1):148–150
71. Yazawa M et al (1992) Effect of one monolayer of surface gold atoms on the epitaxial growth of inas nanowhiskers. Appl Phys Lett 61(17):2051–2053
72. Holmes JD et al (2000) Control of thickness and orientation of solution-grown silicon nanowires. Science 287(5457):1471–1473
73. Nakata M et al (2015) Transfer-free synthesis of highly ordered ge nanowire arrays on glass substrates. Appl Phys Lett 107(13):133102
74. Duan X et al (2001) Indium phosphide nanowires as building blocks for nanoscale electronic and optoelectronic devices. Nature 409(6816):66–69
75. Lindberg C et al (2016) Silver as seed-particle material for gaas nanowires—dictating crystal phase and growth direction by substrate orientation. Nano Lett 16(4):2181–2188
76. Zhang G et al (2008) Growth and characterization of gap nanowires on Si substrate. J Appl Phys 103(1):014301
77. Zhang Y et al (2014) Self-catalyzed ternary core–shell gaasp nanowire arrays grown on patterned Si substrates by molecular beam epitaxy. Nano Lett 14(8):4542–4547
78. Tateno K et al (2012) VLS growth of alternating InAsP/InP heterostructure nanowires for multiple-quantum-dot structures. Nano Lett 12(6):2888–2893
79. Kriegner D et al (2013) Structural investigation of gainp nanowires using X-ray diffraction. Thin Solid Films 543:100–105
80. Tateno K, Zhang G, Nakano H (2008) Growth of GaInAs/AlInAs heterostructure nanowires for long-wavelength photon emission. Nano Lett 8(11):3645–3650
81. Shindo T et al (2011) GaInAsP/InP lateral-current-injection distributed feedback laser with a-Si surface grating. Opt Express 19(3):1884–1891
82. Zhang Y, Xu H, Wang Q (2010) Ultrathin single crystal zns nanowires. Chem Commun 46 (47):8941–8943

83. Zhang XT et al (2003) Growth and luminescence of zinc-blende-structured ZnSe nanowires by metal-organic chemical vapor deposition. Appl Phys Lett 83(26):5533–5535
84. Yan S et al (2011) Novel regrowth mechanism of CdS nanowire in hydrothermal synthesis. New J Chem 35(2):299–302
85. Wu H et al (2012) Dislocation-driven CdS and CdSe nanowire growth. ACS Nano 6 (5):4461–4468
86. Cho K-S et al (2005) Designing PbSe nanowires and nanorings through oriented attachment of nanoparticles. J Am Chem Soc 127(19):7140–7147
87. Finefrock SW et al (2014) Large-scale solution-phase production of Bi2te3 and PbTe nanowires using Te nanowire templates. Nanoscale 6(14):7872–7876
88. Zettler JK et al (2015) High-temperature growth of GaN nanowires by molecular beam epitaxy: toward the material quality of bulk GaN. Cryst Growth Des 15(8):4104–4109
89. Young Kim H, Park J, Yang H (2003) Synthesis of silicon nitride nanowires directly from the silicon substrates. Chem Phys Lett 372(1–2):269–274
90. Kim HY, Park J, Yang H (2003) Direct synthesis of aligned silicon carbide nanowires from the silicon substrates. Chem Commun (2):256–257
91. Kumar A, Madaria AR, Zhou C (2010) Growth of aligned single-crystalline rutile TiO2 nanowires on arbitrary substrates and their application in dye-sensitized solar cells. J Phys Chem C 114(17):7787–7792
92. Wang X et al (2014) Aligned epitaxial SnO2 nanowires on sapphire: growth and device applications. Nano Lett 14(6):3014–3022
93. Jiang X, Herricks T, Xia Y (2002) CuO nanowires can be synthesized by heating copper substrates in air. Nano Lett 2(12):1333–1338
94. Fanhao Z et al (2004) Large-scale growth of In 2 O 3 nanowires and their optical properties. Nanotechnology 15(5):596
95. Zhang YF et al (1998) Silicon nanowires prepared by laser ablation at high temperature. Appl Phys Lett 72(15):1835–1837
96. Wong YY et al (2005) Controlled growth of silicon nanowires synthesized via solid–liquid–solid mechanism. Sci Technol Adv Mater 6(3–4):330–334
97. Wang C et al (2011) Growth of straight silicon nanowires on amorphous substrates with uniform diameter, length, orientation, and location using nanopatterned host-mediated catalyst. Nano Lett 11(12):5247–5251
98. Treuting RG, Arnold SM (1957) Orientation habits of metal whiskers. Acta Metall 5(10):598
99. Pan ZW et al (2001) Temperature-controlled growth of silicon-based nanostructures by thermal evaporation of SiO powders. J Phys Chem B 105(13):2507–2514
100. Morales AM, Lieber CM (1998) A laser ablation method for the synthesis of crystalline semiconductor nanowires. Science 279(5348):208–211
101. Krause A et al (2015) Comparison of silicon nanowire growth on SiO2 and on carbon substrates. ECS Trans 70(1):69–78
102. Kim J, Ji C, Anderson WA (2004) Silicon nanowire growth at relatively low processing temperature. MRS Online Proceedings Library Archive. 818: p. M11.11.1 (6 pages).
103. Cheng SL, Chung CH, Lee HC (2007) Fabrication of vertically aligned silicon nanowire arrays and investigation on the formation of the nickel silicide nanowires. Electron Devices and Solid-State Circuits, 2007. EDSSC 2007. IEEE Conference. pp 121–124.
104. Banerjee D et al (2016) Phonon processes in vertically aligned silicon nanowire arrays produced by low-cost all-solution galvanic displacement method. Appl Phys Lett 108 (11):113109
105. Sandulova AV, Bogoyavlenskii PS, Dronyum MI (1964) Preparation and some properties of whisker and needle-shaped single crystals of germanium, silicon and their solid solutions. Sov Phys Solid State 5:1883
106. Kennedy T et al (2014) High-performance germanium nanowire-based lithium-ion battery anodes extending over 1000 cycles through in situ formation of a continuous porous network. Nano Lett 14(2):716–723

107. Wang D et al (2003) Germanium nanowire field-effect transistors with SiO2 and High-κ Hfo2 gate dielectrics. Appl Phys Lett 83(12):2432–2434
108. Zhang Y et al (2007) An integrated phase change memory cell with Ge nanowire diode for cross-point memory. In 2007 I.E. Symposium on VLSI Technology, 12 Jun, pp 98–99
109. O'Regan C et al (2014) Recent advances in the growth of germanium nanowires: synthesis, growth dynamics and morphology control. J Mater Chem C 2(1):14–33
110. He Y et al (2005) Vertically well-aligned ZnO nanowires generated with self-assembling polymers. Mater Chem Phys 94(1):29–33
111. Yuan Z-Y, Su B-L (2004) Titanium oxide nanotubes, nanofibers and nanowires. Colloids Surf A Physicochem Eng Asp 241(1–3):173–183
112. Shi J, Wang X (2011) Growth of rutile titanium dioxide nanowires by pulsed chemical vapor deposition. Cryst Growth Des 11(4):949–954
113. Faruque MK et al (2012) Fabrication, characterization, and mechanism of vertically aligned titanium nitride nanowires. Appl Surf Sci 260:36–41
114. Wang X et al (2015) Confined-space synthesis of single crystal TiO(2) nanowires in atmospheric vessel at low temperature: a generalized approach. Sci Rep 5:8129
115. Yin Y, Zhang G, Xia Y (2002) Synthesis and characterization of MgO nanowires through a vapor-phase precursor method. Adv Funct Mater 12(4):293–298
116. Zhang Y et al (2001) A simple method to synthesize Si3N4 and SiO2 nanowires from Si or Si/SiO2 mixture. J Cryst Growth 233(4):803–808
117. Xiao Z et al (2006) High-density, aligned SiO2 nanowire arrays: microscopic imaging of the unique growth style and their ultraviolet light emission properties. J Phys Chem B 110 (32):15724–15728
118. Chang C-C et al (2012) Synthesis and growth twinning of Al2O3 nanowires by simple evaporation of Al-Si alloy powder. CrstEngComm 14(3):1117–1121
119. Dang TTL, Tonezzer M, Nguyen VH (2015) Hydrothermal growth and hydrogen selective sensing of nickel oxide nanowires. J Nanomater 2015:8
120. Das S et al (2010) Formation of NiO nanowires on the surface of nickel strips. J Alloys Compd 505(1):L19–L21
121. Lin Y et al (2003) Ordered nickel oxide nanowire arrays and their optical absorption properties. Chem Phys Lett 380(5–6):521–525
122. Pang H et al (2010) Selective synthesis of nickel oxide nanowires and length effect on their electrochemical properties. Nanoscale 2(6):920–922
123. Patil RA et al (2013) An efficient methodology for measurement of the average electrical properties of single one-dimensional NiO nanorods. Sci Rep **3**:3070
124. Sekiya K et al (2012) Morphology control of nickel oxide nanowires. Microelectron Eng 98:532–535
125. Wei ZP et al (2010) A template and catalyst-free metal-etching-oxidation method to synthesize aligned oxide nanowire arrays: NiO as an example. ACS Nano 4(8):4785–4791
126. Zeng W et al (2012) Facile synthesis of NiO nanowires and their gas sensing performance. Trans Nonferrous Met Soc Chin 22:s100–s104
127. Bechelany M et al (2007) Synthesis of boron nitride nanotubes by a template-assisted polymer thermolysis process. J Phys Chem C 111(36):13378–13384
128. Cao L et al (2002) Synthesis of well-aligned boron nanowires and their structural stability under high pressure. J Phys Condens Matter 14(44):11017
129. Cao LM et al (2001) Well-aligned boron nanowire arrays. Adv Mater 13(22):1701–1704
130. Deepak FL et al (2002) Boron nitride nanotubes and nanowires. Chem Phys Lett 353 (5–6):345–352
131. Huo KF et al (2002) Synthesis of boron nitride nanowires. Appl Phys Lett 80(19):3611–3613
132. Kalay S et al (2015) Synthesis of boron nitride nanotubes and their applications. Beilstein J Nanotechnol 6:84–102
133. Patel RB, Chou T, Iqbal Z (2015) Synthesis of boron nanowires, nanotubes, and nanosheets. J Nanomater 2015:7

134. Su C-H et al (2015) Self-templating noncatalyzed synthesis of monolithic boron nitride nanowires. RSC Adv 5(92):75810–75816
135. Zhou J et al (2014) Vertically-aligned BCN nanotube arrays with superior performance in electrochemical capacitors. Sci Rep 4:6083
136. Zhu Y-C et al (2004) New boron nitride whiskers: showing strong ultraviolet and visible light luminescence. J Phys Chem B 108(20):6193–6196
137. Polleux J et al (2006) Template-free synthesis and assembly of single-crystalline tungsten oxide nanowires and their gas-sensing properties. Angew Chem 118(2):267–271
138. An G-H et al (2011) One-pot fabrication of hollow SiO2 nanowires via an electrospinning technique. Mater Lett 65(15–16):2377–2380
139. Antonio T et al (2010) Scalable flame synthesis of SiO 2 nanowires: dynamics of growth. Nanotechnology 21(46):465604
140. Zamchiy A, Baranov E, Khmel S (2014) New approach to the growth of SiO2 nanowires using Sn catalyst on Si substrate. physica status solidi (c) 11(9–10):1397–1400
141. Li Y et al (2011) Growth of SiO 2 nanowires on different substrates using Au as a catalyst. J Semiconduct 32(2):023002
142. Yu-Chiao L, Wen-Tai L (2005) Growth of SiO 2 nanowires without a catalyst via carbothermal reduction of CuO powders. Nanotechnology 16(9):1648
143. Mihailovic D (2009) Inorganic molecular wires: physical and functional properties of transition metal chalco-halide polymers. Prog Mater Sci 54(3):309–350
144. Daniel V et al (2004) Air-stable monodispersed Mo 6 S 3 I 6 nanowires. Nanotechnology 15 (5):635
145. Potel M et al (1980) New pseudo-one-dimensional metals: M2Mo6Se6 (M = Na, in, K, Ti), M2Mo6S6 (M = K, Rb, Cs), M2Mo6Te6 (M = in, Ti). J Solid State Chem 35(2):286–290
146. Remskar M et al (2010) The Mos2 nanotubes with defect-controlled electric properties. Nanoscale Res Lett 6(1):1–6
147. Dvorsek D et al (2007) Growth and field emission properties of vertically aligned molybdenum–sulfur–iodine nanowires on molybdenum and quartz substrates. J Appl Phys 102(11):114308
148. Messer B, Song JH, Yang P (2000) Microchannel networks for nanowire patterning. J Am Chem Soc 122(41):10232–10233
149. Wu Y et al (2002) Inorganic semiconductor nanowires: rational growth, assembly, and novel properties. Chemistry A 8(6):1260–1268
150. Chen H et al (2010) Controlled growth and modification of vertically-aligned carbon nanotubes for multifunctional applications. Mater Sci Eng R Rep 70(3–6):63–91
151. Patole SP et al (2008) Alignment and wall control of ultra long carbon nanotubes in water assisted chemical vapour deposition. J Phys D Appl Phys 41(15):155311
152. Chhowalla M et al (2001) Field emission from short and stubby vertically aligned carbon nanotubes. Appl Phys Lett 79(13):2079–2081
153. Shang NG et al (2010) High-rate low-temperature growth of vertically aligned carbon nanotubes. Nanotechnology 21(50):505604
154. Ago H et al (2011) Ultrahigh-vacuum-assisted control of metal nanoparticles for horizontally aligned single-walled carbon nanotubes with extraordinary uniform diameters. J Phys Chem C 115(27):13247–13253
155. Almaqwashi AA et al (2011) Variable-force microscopy for advanced characterization of horizontally aligned carbon nanotubes. Nanotechnology 22(27):275717
156. Cui R et al (2010) Comparison between copper and iron as catalyst for chemical vapor deposition of horizontally aligned ultralong single-walled carbon nanotubes on silicon substrates. J Phys Chem C 114(37):15547–15552
157. Ding L et al (2009) Selective growth of well-aligned semiconducting single-walled carbon nanotubes. Nano Lett 9(2):800–805
158. Ding L, Yuan D, Liu J (2008) Growth of high-density parallel arrays of long single-walled carbon nanotubes on quartz substrates. J Am Chem Soc 130(16):5428–5429

159. Hong SW, Banks T, Rogers JA (2010) Improved density in aligned arrays of single-walled carbon nanotubes by sequential chemical vapor deposition on quartz. Adv Mater 22 (16):1826–1830
160. Huang L et al (2006) Cobalt ultrathin film catalyzed ethanol chemical vapor deposition of single-walled carbon nanotubes. J Phys Chem B 110(23):11103–11109
161. Huang S et al (2004) Growth mechanism of oriented long single walled carbon nanotubes using "fast-heating"chemical vapor deposition process. Nano Lett 4(6):1025–1028
162. Inoue T et al. High density growth of horizontally aligned single-walled carbon nanotubes on quartz by variation of incubation time. http://www.photon.t.u-tokyo.ac.jp/~maruyama/papers/12/DenseHA.pdf
163. Ismach A, Kantorovich D, Joselevich E (2005) Carbon nanotube graphoepitaxy: highly oriented growth by faceted nanosteps. J Am Chem Soc 127(33):11554–11555
164. Kang SJ et al (2007) High-performance electronics using dense, perfectly aligned arrays of single-walled carbon nanotubes. Nat Nanotechnol 2(4):230–236
165. Kocabas C et al (2005) Guided growth of large-scale, horizontally aligned arrays of single-walled carbon nanotubes and their use in thin-film transistors. Small 1(11):1110–1116
166. Ozel T et al (2009) Nonuniform compressive strain in horizontally aligned single-walled carbon nanotubes grown on single crystal quartz. ACS Nano 3(8):2217–2224
167. Reina A et al (2007) Growth mechanism of long and horizontally aligned carbon nanotubes by chemical vapor deposition. J Phys Chem C 111(20):7292–7297
168. Shadmi N et al (2015) Guided growth of horizontal single-wall carbon nanotubes on M-plane sapphire. J Phys Chem C 119(15):8382–8387
169. Yu Q et al (2006) Mechanism of horizontally aligned growth of single-wall carbon nanotubes on R-plane sapphire. J Phys Chem B 110(45):22676–22680
170. Yuan D et al (2008) Horizontally aligned single-walled carbon nanotube on quartz from a large variety of metal catalysts. Nano Lett 8(8):2576–2579
171. Zhou W et al (2006) Copper catalyzing growth of single-walled carbon nanotubes on substrates. Nano Lett 6(12):2987–2990
172. AuBuchon JF et al (2006) Electric-field-guided growth of carbon nanotubes during DC plasma-enhanced CVD. Chem Vap Deposition 12(6):370–374
173. Chai Y, Xiao Z, Chan PCH (2009) Fabrication and characterization of horizontally aligned carbon nanotubes for interconnect application. 2009 59th electronic components and technology conference, San Diego, CA, May 2009. pp 1465–1469
174. Chai Y, Xiao Z, Chan PCH (2010) Horizontally aligned carbon nanotube bundles for interconnect application: diameter-dependent contact resistance and mean free path. Nanotechnology 21(23):235705
175. Hayashi Y et al (2010) Direct growth of horizontally aligned carbon nanotubes between electrodes and its application to field-effect transistors. 2010 3rd international nanoelectronics conference (INEC). pp 215–216
176. Joselevich E, Lieber CM (2002) Vectorial growth of metallic and semiconducting single-wall carbon nanotubes. Nano Lett 2(10):1137–1141
177. Jung SM, Jung HY, Suh JS (2007) Horizontally aligned carbon nanotube field emitters having a long term stability. Carbon 45(15):2917–2921
178. Jung SM, Jung HY, Suh JS (2008) Horizontally aligned carbon nanotube field emitters fabricated on ITO glass substrates. Carbon 46(14):1973–1977
179. Law JBK, Koo CK, Thong JTL (2007) Horizontally directed growth of carbon nanotubes utilizing self-generated electric field from plasma induced surface charging. Appl Phys Lett 91(24):243108
180. Ural A, Li Y, Dai H (2002) Electric-field-aligned growth of single-walled carbon nanotubes on surfaces. Appl Phys Lett 81(18):3464–3466
181. Zhang Y et al (2001) Electric-field-directed growth of aligned single-walled carbon nanotubes. Appl Phys Lett 79(19):3155–3157

182. Ago H et al (2006) Synthesis of horizontally-aligned single-walled carbon nanotubes with controllable density on sapphire surface and polarized raman spectroscopy. Chem Phys Lett 421(4–6):399–403
183. Hong BH et al (2005) Quasi-continuous growth of ultralong carbon nanotube arrays. J Am Chem Soc 127(44):15336–15337
184. Hsu CM et al (2002) Growth of the large area horizontally-aligned carbon nanotubes by ECR-CVD. Thin Solid Films 420–421:225–229
185. Huang S, Cai X, Liu J (2003) Growth of millimeter-long and horizontally aligned single-walled carbon nanotubes on flat substrates. J Am Chem Soc 125(19):5636–5637
186. Jin Z et al (2007) Ultralow feeding gas flow guiding growth of large-scale horizontally aligned single-walled carbon nanotube arrays. Nano Lett 7(7):2073–2079
187. Li L et al (2012) Electrochemical growth of gold nanoparticles on horizontally aligned carbon nanotubes: a new platform for ultrasensitive DNA sensing. Biosens Bioelectron 33(1):279–283
188. Liu H et al (2009) The controlled growth of horizontally aligned single-walled carbon nanotube arrays by a gas flow process. Nanotechnology 20(34):345604
189. Liu Y et al (2009) Flexible orientation control of ultralong single-walled carbon nanotubes by gas flow. Nanotechnology 20(18):185601
190. Xie H et al (2016) Preloading catalysts in the reactor for repeated growth of horizontally aligned carbon nanotube arrays. Carbon 98:157–161
191. Dayeh SA, Picraux ST (2010) Direct observation of nanoscale size effects in ge semiconductor nanowire growth. Nano Lett 10(10):4032–4039
192. Qi H et al (2012) Growth of vertically aligned ZnO nanowire arrays using bilayered metal catalysts. J Nanomater 2012:7
193. Fengmei G et al (2008) Aligned ultra-long single-crystalline A—Si 3 N 4 nanowires. Nanotechnology 19(10):105602
194. Woodruff JH et al (2007) Vertically oriented germanium nanowires grown from gold colloids on silicon substrates and subsequent gold removal. Nano Lett 7(6):1637–1642
195. Toko K et al (2015) Vertically aligned Ge nanowires on flexible plastic films synthesized by (111)-oriented Ge seeded vapor–liquid–solid growth. ACS Appl Mater Interfaces 7 (32):18120–18124
196. Sierra-Sastre Y et al (2008) Vertical growth of Ge nanowires from biotemplated Au nanoparticle catalysts. J Am Chem Soc 130(32):10488–10489
197. O'Regan C et al (2013) Engineering the growth of germanium nanowires by tuning the supersaturation of Au/Ge binary alloy catalysts. Chem Mater 25(15):3096–3104
198. Li CB et al (2008) Controlled Ge nanowires growth on patterned Au catalyst substrate. 2008 I.E. silicon nanoelectronics workshop, pp 1–2
199. Leu PW et al (2008) Oxide-encapsulated vertical germanium nanowire structures and their DC transport properties. Nanotechnology 19(48):485705
200. Kawamura Y et al (2012) Direct-gap photoluminescence from germanium nanowires. Physical Review B **86**(3):035306
201. Liangbing H, Hecht DS, Grüner G (2009) Infrared transparent carbon nanotube thin films. Appl Phys Lett 94(8):081103. (3 pp)
202. Adhikari H et al (2006) Germanium nanowire epitaxy: shape and orientation control. Nano Lett 6(2):318–323
203. Geng C et al (2004) Well-aligned ZnO nanowire arrays fabricated on silicon substrates. Adv Funct Mater 14(6):589–594
204. Jamali Sheini F et al (2010) Low temperature growth of aligned ZnO nanowires and their application as field emission cathodes. Mater Chem Phys 120(2–3):691–696
205. Ji L-W et al (2009) Effect of seed layer on the growth of well-aligned ZnO nanowires. J Phys Chem Solid 70(10):1359–1362
206. Liu F et al (2005) Well-aligned zinc oxide nanorods and nanowires prepared without catalyst. J Cryst Growth 274(1–2):126–131

207. Tak Y, Yong K (2005) Controlled growth of well-aligned ZnO nanorod array using a novel solution method. J Phys Chem B 109(41):19263–19269
208. Unalan HE et al (2008) Rapid synthesis of aligned zinc oxide nanowires. Nanotechnology 19 (25):255608
209. Xu S et al (2008) Patterned growth of vertically aligned ZnO nanowire arrays on inorganic substrates at low temperature without catalyst. J Am Chem Soc 130(45):14958–14959
210. Zeng Y-J et al (2005) Well-aligned ZnO nanowires grown on Si substrate via metal–organic chemical vapor deposition. Appl Surf Sci 250(1–4):280–283
211. Zhitao H et al (2013) Controlled growth of well-aligned ZnO nanowire arrays using the improved hydrothermal method. J Semiconduct 34(6):063002
212. Lin W et al (2009) Vertically aligned carbon nanotubes on copper substrates for applications as thermal interface materials: from synthesis to assembly. 2009 59th electronic components and technology conference, pp 441–447
213. Qi HJ et al (2003) Determination of mechanical properties of carbon nanotubes and vertically aligned carbon nanotube forests using nanoindentation. J Mech Phys Solids 51 (11–12):2213–2237
214. Qu L, Du F, Dai L (2008) Preferential syntheses of semiconducting vertically aligned single-walled carbon nanotubes for direct use in FETs. Nano Lett 8(9):2682–2687
215. Ren ZF et al (1998) Synthesis of large arrays of well-aligned carbon nanotubes on glass. Science 282(5391):1105–1107
216. Shahzad MI et al (2013) Growth of vertically aligned multiwall carbon nanotubes columns. J Phys Conf Ser 439(1):012008
217. Van Hooijdonk E et al (2013) Functionalization of vertically aligned carbon nanotubes. Beilstein J Nanotechnol 4:129–152
218. Yu M et al (2009) High density, vertically-aligned carbon nanotube membranes. Nano Lett 9 (1):225–229
219. Zhu H et al (2001) Hydrogen adsorption in bundles of well-aligned carbon nanotubes at room temperature. Appl Surf Sci 178(1–4):50–55
220. Remškar DVM et al (2004) Air-stable monodispersed Mo 6 S 3 I 6 nanowires. Nanotechnology 15(5):635
221. Zhang Z et al (2015) Ultrathin inorganic molecular nanowire based on polyoxometalates. Nat Commun 6

Chapter 2
Taxane Formulations: From Plant to Clinic

A. Elhissi, R. Mahmood, I. Parveen, A. Vali, W. Ahmed, and M.J. Jackson

2.1 Plant Origin and Pharmacology of Taxanes

Taxane compounds are anticancer agents derived from a plant source and include paclitaxel and docetaxel (Fig. 2.1). Paclitaxel is isolated from the Pacific yew tree (*Taxus brevifolia*) [1], whilst the semisynthetic taxane docetaxel is derived from the needles of the European yew (*Taxus baccata*) [2, 3]. Taxane formulations can treat various types of cancer including ovarian, breast and bladder carcinomas [4] as well as lung cancer and acute leukaemia [2].

Taxanes are classified as anti-microtubule chemotherapeutic compounds that work by interrupting the microtubule function which is important in cell division. They do so by inhibiting mitosis, causing an incomplete formation of the metaphase plate of chromosomes and hence altering the arrangement of the spindle microtubules [5, 6]. Both paclitaxel and docetaxel bind to ß subunit of tubulin (a protein found in microtubules) [7, 8], producing highly stable dysfunctional microtubules [9]. Microtubules are central to cell division forming spindle fibres permitting separation and alignment of chromosomes during mitosis [10]. Paclitaxel inhibits mitosis in the G-phase of the mitotic cycle, whilst docetaxel causes arrest at the

A. Elhissi (✉)
College of Pharmacy, Qatar University, Doha, Qatar
e-mail: aelhissi@qu.edu.qa

R. Mahmood • I. Parveen • A. Vali
School of Pharmacy and Biomedical Sciences, University of Central Lancashire, Preston PR1 2HE, UK

W. Ahmed
School of Mathematics and Physics, University of Lincoln, Lincoln LN6 7TS, UK

M.J. Jackson
School of Interdisciplinary Studies, Kansas State University, Manhattan, KS 66506, USA

M.J. Jackson, W. Ahmed (eds.), *Micro and Nanomanufacturing Volume II*,
DOI 10.1007/978-3-319-67132-1_2

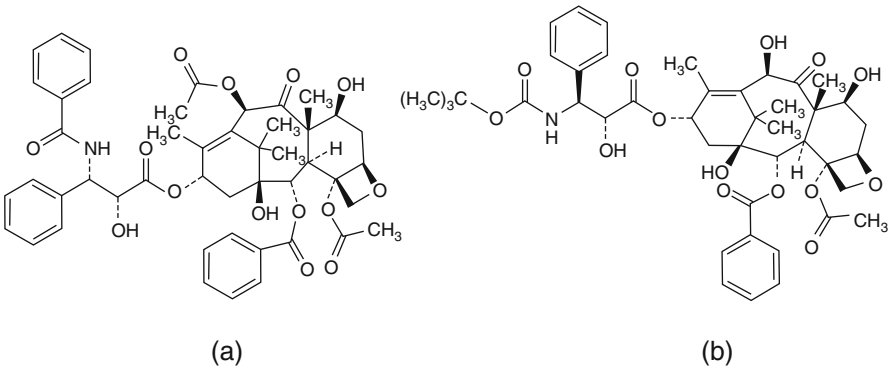

Fig. 2.1 Chemical structure of (**a**) paclitaxel and (**b**) docetaxel

S-phase to prevent cell division and produce apoptosis [11]. Docetaxel has been reported to be twice as potent as paclitaxel at inhibiting microtubules [12].

2.2 Conventional Taxane Formulations in Clinical Use

Paclitaxel and docetaxel are highly lipophilic; hence, they are both regarded to be water-insoluble compounds (Table 2.1), making formulation and administration considerably challenging. Paclitaxel is solubilised using a mixture of Cremophor EL (polyethoxylated castor oil) and dehydrated ethanol (50:50 v/v) to provide a drug concentration of 6 mg/mL [13, 14]. Cremophor EL is a non-ionic surfactant that has the ability to form micelles in biological fluids (e.g. plasma) and increase the solubility of paclitaxel. By contrast, docetaxel is slightly more soluble than paclitaxel; therefore polysorbate 80 (Tween 80) and ethanol are used to solubilise it [15, 16]. These paclitaxel and docetaxel formulations are available for clinical use as Taxol® and Taxotere®, respectively, and are administered by intravenous infusion. Before administration of Taxol®, the formulation is diluted with 5–20-fold using NaCl (0.9%) or dextrose (5%) solutions [9].

2.3 Stability of Taxane Formulations

Stability of taxane is extremely important particularly in situations where chemotherapy is prepared for later administration [17]. In these cases, storage conditions may affect the drug dose received. Docetaxel stability can be influenced by the degree of agitation during preparation and by slight temperature fluctuations during storage [18]. By contrast, for paclitaxel, the optimum storage temperature was